

IET Renewable Power Generation

Special Issue Call for Papers

**Be Seen. Be Cited.
Submit your work to a new
IET special issue**

Connect with researchers and
experts in your field and
share knowledge.




Be part of the latest research
trends, faster.

[Read more](#)



The Institution of
Engineering and Technology

Power maximising control of a heaving point absorber wave energy converter

Yifeng Gu  | Boyin Ding  | Nataliia Y. Sergiienko  | Benjamin S. Cazzolato

School of Mechanical Engineering, The University of Adelaide, Adelaide, South Australia, Australia

Correspondence

Boyin Ding, School of Mechanical Engineering, The University of Adelaide, Adelaide, South Australia, 5005.

Email: boyin.ding@adelaide.edu.au

Abstract

Control systems play a critical role in improving the economic viability of wave energy converters (WEC). This paper presents a framework for a causal power-maximising feedback controller inspired by Phi method. Quadratic damper control and PID control are combined to collectively achieve the optimal power absorption conditions for the peak wave periods, which results in a nonlinear controller being suboptimal in irregular waves. The proposed controller is tested on a fully submerged heaving spherical point absorber in regular and irregular wave conditions in time domain. The tuning of the PID gains are investigated in frequency-domain from a stability and control bandwidth perspective. The modelled WEC dynamics includes linear hydrodynamic forces (excitation and radiation) and the nonlinear viscous drag force. The main benefits of the proposed controller are (i) it does not require any time-consuming optimisation either online or offline; (ii) has a wider bandwidth and better power absorption performance as compared to the conventional spring-damper (PI) controller; and (iii) easy to implement in practice like standard PID control.

1 | INTRODUCTION

A wave energy converter (WEC) is a device that converts ocean wave energy into useful electricity. Compared with other renewable energy sources such as solar or wind, the main challenge in commercialising WEC technologies remains in reducing their costs, which needs to take into consideration manufacturing, installation, and maintenance [1]. One of the critical and major pathways for improving the economic viability of wave energy is seen in the design of better controllers [2].

It is well-known that the maximum power absorption of a WEC in regular waves can be achieved using complex-conjugate control (CCC), also known as impedance matching control [3]. CCC effectively describes the underlying dynamics behind maximum energy absorption, however, it has some difficulties in practical application [4]. In order for CCC to be successful in irregular waves and provide perfect impedance-matching across all frequencies, it is required to predict the system dynamics for some time in the future leading to the acausality problem [5]. Acausal controllers (i.e. model predictive control [6]) heavily rely on prediction/estimation of the future incoming waves, and the accuracy of the WEC model. Despite some success in accurately

predicting wave elevations [7] and testing acausal controllers in laboratory environment [8], they are difficult and computationally expensive to implement in real life.

It is possible to avoid the acausality issue in the WEC control design if the impedance matching is achieved not across all frequencies simultaneously, but covering only a limited range of dominant wave frequencies. Controllers built using this philosophy are sub-optimal in irregular waves but can produce power close to optimal conditions [9]. There are a number of ways to design a causal approximation of CCC leading to simple and reliable control strategies. The most widely used control law for point absorbing WECs is a spring-damper controller, sometimes called proportional–integral (PI), using WEC velocity as a basis, where stiffness and damping coefficients are tuned to achieve impedance matching at one dominant frequency [10]. Depending on the WEC dynamics and considered sea states, PI control can achieve up to 77–93% of the theoretical power limit [9]. As PI control is narrow-banded by nature and optimal for one wave condition only, a self-tuning PI strategy, where control parameters are adjusted in real-time according to the wave environment, has been tested in [11]. Another way to approximate CCC has been proposed in [12, 13], where multiple

This is an open access article under the terms of the [Creative Commons Attribution](https://creativecommons.org/licenses/by/4.0/) License, which permits use, distribution and reproduction in any medium, provided the original work is properly cited.

© 2021 The Authors. *IET Renewable Power Generation* published by John Wiley & Sons Ltd on behalf of The Institution of Engineering and Technology

parallel PI controllers act simultaneously targeting individual wave frequencies from the wave spectrum. Such controllers require a real-time decomposition of the displacement or velocity time-series into multiple frequency components using Fast Fourier Transforms or least squares methods in real time.

In the PI (spring-damper) control algorithms, the integral (stiffness) control coefficient is usually tuned to effectively cancel out the total intrinsic reactance of the WEC containing its mass/inertia and hydrostatic stiffness via resonance [3]. Alternatively, [6] proposed a PID (mass-spring-damper) control structure that uses two separate control terms to cancel out the intrinsic mass/inertia (acceleration feedback) and stiffness (displacement feedback) correspondingly. This PID control (termed as approximate CCC in [6]) demonstrates a performance close to the model-predictive control strategy (10–25% absorbed power reduction); however, its coefficients should be carefully tuned to avoid system instability and maintain sufficient stability margin [14].

The concept of CCC usually requires that the wave energy converter has linear dynamics, and control parameters are tuned based on the hydrodynamic coefficients. Once the height of the incoming wave increases, nonlinear effects such as the viscous drag force start affecting the WEC motion and power output [15]. To account for nonlinear dynamics in the controller design, the WEC model is usually linearised and control parameters are optimised to achieve maximum power absorption for the sea states of interests [16]. Similarly, many recently developed optimal controllers such as bang-bang based controller are applicable only when a linear dynamics model is valid despite their capability to handle constraints [17]. To address both linear and nonlinear dynamics in WEC power maximising control, an alternative approach, termed Phi method, has been proposed in [18], where the optimal control force is formulated analytically based on the known dynamics of the WEC, linear or nonlinear.

Inspired by previous work on WEC PID control and Phi method, this paper proposes and investigates a novel causal power maximising controller, termed as PP²ID (mass-spring-linear/quadratic damper) control, on a fully submerged heaving point absorber. Quadratic damper control and PID control are combined to collectively achieve the optimal power absorption conditions for the peak wave periods, which results in a nonlinear controller that is suboptimal in irregular waves. The main contributions of this paper are: (i) tuning of the proposed controller (after linearisation) is investigated analytically in the frequency domain from a stability and control bandwidth perspective; (ii) power performance of the proposed controller is studied for both regular and irregular waves using time-domain simulations; (iii) although the concept of WEC PID control is not entirely new, its application to a fully submerged point absorber is original, and its integration with quadratic damper control to account for nonlinear viscous drag effects is unique. The structure of the paper is as follows below. Section 2 covers the modelling of the WEC system. Section 3 shows the controller design concepts, including simulation methodology. Section 4 demonstrates the stability and control bandwidth analysis obtained in frequency domain. Section 5 demonstrates the

power performance analysis obtained in time domain. The last section concludes the main contributions of the paper.

2 | WAVE ENERGY CONVERTER

2.1 | Mathematical model in time domain

Linear wave theory is commonly used to estimate the hydrodynamic forces acting on a structure, where the dynamic equation of motion can be formulated in either the frequency or time domain. Equation (1) describes the motion of a WEC (e.g. in one degree of freedom) under the wave excitation:

$$m\ddot{\zeta}(t) = F_{\text{exc}}(t) + F_{\text{rad}}(t) + F_{\text{pto}}(t) + F_{\text{hs}}(t) + F_{\text{vis}}(t), \quad (1)$$

where m is the mass of the buoy; ζ is the buoy displacement in heave; F_{exc} is the excitation force; F_{rad} is the wave radiation force; F_{pto} is the control force acting on the buoy from the PTO unit; F_{hs} is the hydrostatic force; and F_{vis} is the viscous drag force, modelled according to the Morison equation [19]: $F_{\text{vis}}(t) = -\frac{1}{2}\rho C_{\text{D}}A_{\text{D}}|\dot{\zeta} - \dot{\zeta}_0|(\dot{\zeta} - \dot{\zeta}_0)$, where ρ is the density of water, C_{D} is the drag coefficient, A_{D} is the cross-sectional area of buoy perpendicular to the incident wave, and $\dot{\zeta}_0$ is the fluid velocity at the centre of mass of the buoy undisturbed which is assumed to be negligible compared to the buoy velocity in this paper.

The most common mathematical model that describes a time-domain response of a WEC excited by waves is the Cummins equation [20]:

$$(m + A_{\infty})\ddot{\zeta}(t) + \int_{-\infty}^t B(t - \tau)\dot{\zeta}(\tau) d\tau + \frac{1}{2}\rho C_{\text{D}}A_{\text{D}}|\dot{\zeta}(t)|\dot{\zeta}(t) + F_{\text{hs}}(t) = F_{\text{exc}}(t) + F_{\text{pto}}(t), \quad (2)$$

where A_{∞} is the infinite-frequency added mass coefficient; $B(t)$ is the radiation impulse response function, depending on the motion history of the buoy; F_{hs} is the hydrostatic force. As for a fully submerged buoy case considered in this paper, it is assumed that the net buoyancy force of the buoy is always balanced by a PTO pretension force. Therefore, the hydrostatic force becomes zero. For simulations on the radiation effects in the time-domain, the convolution integral in Equation (2) is replaced by a state-space model according to the methodology presented in [21]. Hydrodynamic parameters of a submerged spherical buoy including the excitation force, and the corresponding frequency-dependent added mass and radiation damping in Equation (2) are calculated using a semi-analytical model developed by [22]. For a spherical buoy, C_{D} is estimated to be 0.5 based on experimental measurement [23] and $A_{\text{D}} = \pi r^2$, where r is the radius of the buoy. In practice, the PTO force is dependent on the PTO machinery design which can be very complex. At the WEC design stage and for simplicity, PTO force is usually assumed to be a linear function of the system state feedback measured by sensors, which will be introduced in the following sections.

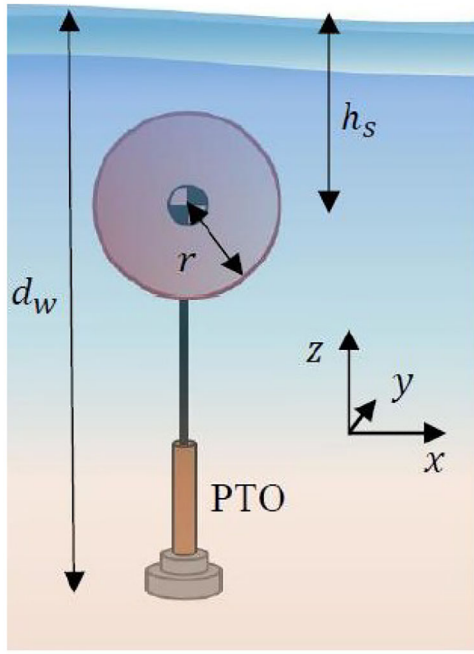


FIGURE 1 Fully submerged 1DOF single tether spherical buoy [24].

TABLE 1 Parameters of a fully submerged spherical buoy

Items	Value/unit
Buoy radius (r)	5 m
Submerged depth (h_s)	8.5 m
Water depth (d_w)	50 m
Buoy mass (m)	2.698×10^5 kg
Water density (ρ)	1024 kg/m ³
Gravitational acceleration (g)	9.8067 m/s ²

2.2 | Description of the WEC system

A heaving fully submerged spherical buoy is used as a typical test case in this study as shown in Figure 1. Table 1 shows corresponding parameters, where r is the radius of the buoy; h_s is the submerged depth, which is the distance from the water surface to the centre of mass of the buoy; d_w is the water depth; m is the mass of buoy and ρ is the density of water; and g is gravitational acceleration.

3 | POWER MAXIMISING CONTROLLER

3.1 | Design of power maximising controller

3.1.1 | Phi method

Mills and Ding [18] studied the mathematical derivation of Phi method, an algorithmic operator that determines the optimal PTO control force in time-domain for maximising WEC power

TABLE 2 Typical dynamic terms and corresponding Phi derived optimal control forces [18]

Dynamic terms	Analytical expression (H)	Phi-derived control force (F_{pto})
Spring	$a_0 z(t)$	$a_0 z(t)$
Damper	$a_1 \dot{z}(t)$	$-a_1 \dot{z}(t)$
Inertia	$a_2 \ddot{z}(t)$	$a_2 \ddot{z}(t)$
Viscous drag	$a_3 \dot{z}(t) \dot{z}(t)$	$-2a_3 \dot{z}(t) \dot{z}(t)$

absorption. The WEC dynamics can be written as the following general expression:

$$H(t; z, \dot{z}, \ddot{z}, \dots, z^{(n)}) = F_{exc}(t) + F_{pto}(t), \quad (3)$$

where $z^{(n)} = \frac{\partial^n z}{\partial t^n}$ and n is the highest order of the time derivatives. H is a sufficiently smooth function of time derivatives describing the WEC dynamics in response to the excitation and PTO control forces, that are not necessarily linear.

Phi method derives the optimal control force as functions of the WEC time response from the analytical WEC dynamics H using the following expression [18]:

$$F_{pto}(t) = -\alpha + \int_0^t \dot{z} \frac{\partial}{\partial z} H d\tau - \sum_{k=1}^{\infty} \left(-\frac{\partial}{\partial t} \right)^{k-1} \left(\dot{z} \frac{\partial}{\partial z^{(k)}} H \right), \quad (4)$$

where α is a bias force equal to the mean wave force that prevents the WEC from drifting. Table 2 shows some typical dynamics terms and their corresponding optimal PTO control force derived using Equation (4). The step-to-step derivation procedures are shown in Appendix A.

Substituting the dynamic expressions and their corresponding Phi-derived control force into Equation (3) and combining/cancelling common terms, the following observations can be made. The system intrinsic spring term and inertia term are respectively cancelled by the corresponding Phi-derived feedback control force, while the linear damper term is doubled by linear damper control. These lead to the optimal force-to-velocity mapping under impedance matching theory for the maximum power absorption of a WEC in [3] assuming the system is linear and under harmonic motion. The viscous drag term, or quadratic damper term, however, according to the Phi method, is tripled by quadratic damper control, which has never been noted in the literature to the best knowledge of the authors. To assist in understanding this outcome, a mathematical proof extended from impedance matching theory is shown in Appendix B.

3.1.2 | Phi-inspired feedback control

The convolution integral in the Cummins equation, Equation (2), depends on the past information of the buoy motion.

Therefore, the corresponding optimal PTO control force depends on the future information of the excitation force, which leads to acausal control [5]. For the derivation of causal feedback controller using the Phi method, the convolution integral in Equation (2) is decomposed into the wave frequency-dependent added mass term and radiation damping term assuming that the WEC reaches its steady-state response and oscillates under periodic waves, e.g. $\eta(t) = A \cos(\omega t + \varphi_n)$ and $\zeta(t) = \zeta_0 \cos(\omega t + \varphi_\zeta)$. Therefore, for a fully submerged point absorber WEC, Equation (2) can be rewritten as:

$$(m + A^\omega) \ddot{\zeta}(t) + B_{\text{rad}}^\omega \dot{\zeta}(t) + \frac{1}{2} \rho C_D A_D |\dot{\zeta}(t)| \dot{\zeta}(t) = F_{\text{exc}}(t) + F_{\text{pto}}(t), \quad (5)$$

where $A^\omega = A(\omega)$ and $B_{\text{rad}}^\omega = B_{\text{rad}}(\omega)$ are the wave frequency-dependent added mass and radiation damping respectively. Denoting the left hand side of Equation (5) as H and the applying Phi-operator using Equation (4), Phi-derived causal feedback control for a fully submerged point absorber WEC can be obtained:

$$F_{\text{pto}}(t) = \underbrace{(m + A^\omega) \ddot{\zeta}(t)}_{\text{Mass control}} - \underbrace{B_{\text{rad}}^\omega \dot{\zeta}(t) - \rho C_D A_D |\dot{\zeta}(t)| \dot{\zeta}(t)}_{\text{Damper control}}, \quad (6)$$

which consists of a mass (or inertia feedback) control term that cancels the system intrinsic mass; a linear damper (or velocity feedback) control term that doubles the radiation damping; and a quadratic damper (or velocity square feedback) control term that triples the viscous drag. The feedback controller in Equation (6) is optimal in regular waves, however, is sub-optimal in irregular waves because the control parameters A^ω and B_{rad}^ω can be tuned at optimal for a single/dominant wave frequency only, leading to a narrow-banded suboptimal controller in nature.

The most well-known and commonly used causal feedback control for maximising WEC power absorption is a spring-damper control law:

$$F_{\text{pto}}(t) = \underbrace{-K_{\text{pto}} \zeta(t)}_{\text{Spring control}} - \underbrace{-B_{\text{pto}} \dot{\zeta}(t)}_{\text{Damper control}}, \quad (7)$$

where K_{pto} and B_{pto} are respectively the stiffness coefficient for the spring (or displacement feedback) control term and the damping coefficient for the linear damper (or velocity feedback) control term. According to principle of complex conjugate control [3] where viscous drag is ignored in the WEC dynamics, the optimal values of K_{pto} and B_{pto} are:

$$K_{\text{pto}} = \omega^2 (m + A(\omega)), \quad (8)$$

$$B_{\text{pto}} = B_{\text{rad}}(\omega), \quad (9)$$

for a fully submerged point absorber WEC. Equations (8) and (9) are respectively the resonance condition and the optimal

amplitude condition that are frequency-dependent. When viscous drag is considered in the WEC dynamics, the optimal amplitude condition becomes:

$$B_{\text{pto}} = B_{\text{rad}}(\omega) + B_{\text{vd}}(\omega), \quad (10)$$

where B_{vd} is an additional linear damper in the PTO accounting for the viscous drag/quadratic damping dynamics $\frac{1}{2} \rho C_D A_D |\dot{\zeta}(t)| \dot{\zeta}(t)$, which is often determined via numerical optimisation approach, and varies with the variation of both wave frequency and wave height.

Substituting Equations (8) and (10) into Equation (7) and comparing to Equation (6) leads to the following observations:

- Spring control cancels the WEC intrinsic mass term including the buoy mass and added mass only at the WEC resonance condition where the spring force is in anti-phase with the system inertia force, whilst mass control directly cancels the WEC intrinsic mass by applying an opposite equal force. Both spring and mass control aim to force the buoy velocity to be in phase with the wave excitation force; however, mass control may raise control instability issue [25], which was not considered by Phi method.
- Linear damper control doubles the WEC intrinsic linear damper terms, including the radiation damping and the linearised viscous drag to achieve the optimal amplitude condition. Phi method further applies quadratic damping control to triple the WEC viscous drag term. The resulting quadratic damping control is nonlinear and optimal regardless of variations in wave frequency and wave height. Therefore, numerical optimisation-based linearisation for linear damper control is no longer necessary.

To gain a comprehensive understanding on the performance of spring and mass control strategies in combination with linear damper control, a linear mass-spring-damper controller (or more generally termed PID controller in control discipline) is applied [26]:

$$F_{\text{pto}}^{\text{PID}}(t) = \underbrace{a(m + A^\omega) \ddot{\zeta}(t)}_{\text{Derivative (mass control)}} - \underbrace{b\omega^2 (m + A^\omega) \zeta(t)}_{\text{Integral (spring control)}} \quad (11)$$

$$- \underbrace{(B_{\text{rad}}^\omega + B_{\text{vd}}^\omega) \dot{\zeta}(t)}_{\text{Proportional (linear damper control)}}, \quad (11)$$

where $\dot{\zeta}(t)$ is regarded as the system output and thus with respect to the system output linear damper (or velocity feedback) control denotes the proportion term (P), spring (or displacement feedback) control denotes the integral term (I), and mass (or inertia feedback) control denotes the derivative term (D). The terms a and b in Equation (11) are respectively the ratios of the D term (mass control) and I term (spring control), which are defined for understanding the transitions between pure spring and pure mass control. To satisfy the WEC resonance condition under partial mass control $0 < a < 1$ and

partial spring control $0 < b < 1$, the constraint $a + b = 1$ is required to be met. In extreme case when $a = 0$ & $b = 1$, Equation (11) becomes pure PI control (or linear spring-damper control) in Equation (7). On the other hand, when $a = 1$ & $b = 0$, Equation (11) becomes pure PD control (or linear mass-damper control).

Inspired by Phi method, a quadratic damping control is integrated into the PID controller that leads to a novel nonlinear PP²ID controller:

$$F_{\text{pto}}^{\text{PP}^2\text{ID}}(t) = \underbrace{a(m + A^\omega) \ddot{\chi}(t)}_{\text{D (mass control)}} - \underbrace{b\omega^2(m + A^\omega)\chi(t)}_{\text{I (spring control)}} \quad (12)$$

$$\underbrace{-B_{\text{rad}}^\omega \dot{\chi}(t)}_{\text{P (linear damper control)}} - \underbrace{\rho C_D A_D |\dot{\chi}(t)| \dot{\chi}(t)}_{\text{P}^2 \text{ (quadratic damper control)}}, \quad (12)$$

where the quadratic damper (or velocity squared feedback) control denotes the nonlinear proportional square term (P²). Since control parameters of PID control in Equation (11) and PP²ID control in Equation (12) are frequency-dependent, both controllers are optimal in regular waves at a particular wave period. In irregular waves, both controllers are sub-optimal and thus their control parameters are often tuned according to the energy period of the wave spectrum (detailed in Section 5). It is worth noting that the P gain of the PID control in Equation (11) usually needs to be determined via a numerical optimisation to account for the nonlinear viscous drag dynamics, whereas the optimal control parameters of PP²ID control in Equation (12) can be analytically determined due to the use of quadratic damper control. For both controllers, the optimal ratio between the D gain (a) and the I gain (b) need to be initially investigated. This is assisted by the frequency-domain analysis on the PID controller configuration in Section 4, with the results equally applicable to the PP²ID controller.

4 | PID CONFIGURATION ANALYSIS IN FREQUENCY DOMAIN

4.1 | Transfer function of WEC feedback control system

Frequency-domain approach is often used to investigate and tune the performance of feedback control from a stability and control bandwidth perspective [9]. Substituting the PID control force in Equation (11) into the WEC equation of periodic motion (under harmonic oscillation) in Equation (5), and applying Lorenz linearisation [27] to approximate the nonlinear viscous drag effects following that in [28, 29], the linearised model of the WEC feedback control system is obtained. The objective of Lorenz linearisation is to find a linearised damping force (e.g. a frequency-dependent damping coefficient B_{vd}^ω) that dissipates the same amount of energy as the nonlinear quadratic force in regular waves under PI _{b} D _{a} control. An iterative procedure is implemented to calculate B_{vd}^ω , because B_{vd}^ω determines the P gain of the controller in Equation (11) while

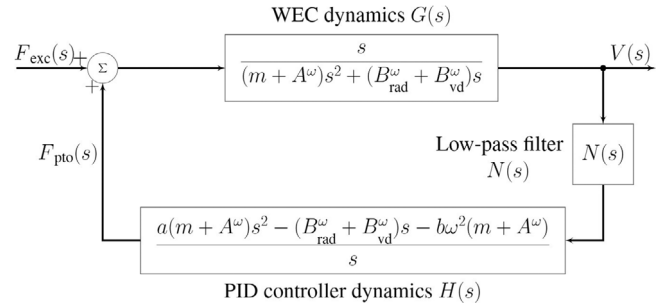


FIGURE 2 Block diagram of WEC feedback control system

B_{vd}^ω is determined by the control force under Lorenz linearisation. It is worth noting the inclusion of this linearised version of the drag is critical for the frequency-domain analysis, since it significantly affects the phase margin of the WEC feedback control system.

Then applying the Laplace transform to the resulting linear model in the time-domain following the approach in [14], the closed-loop transfer function (CLTF) describing the force-to-velocity mapping of the WEC system under PI _{b} D _{a} control is obtained:

$$\frac{V(s)}{F_{\text{exc}}(s)} = \frac{G(s)}{1 - G(s)H(s)} = \frac{G(s)}{(1-a)(m + A^\omega)s^2 + 2(B_{\text{rad}}^\omega + B_{\text{vd}}^\omega)s + b\omega^2(m + A^\omega)}, \quad (13)$$

where $V(s)$ denotes the Laplace transform of the buoy velocity; $G(s)$ denotes the WEC dynamics and $H(s)$ denotes the PID controller dynamics, whose TFs are respectively shown in Figure 2. $N(s)$ on the feedback of the closed-loop system in Figure 2 represents a low-pass filter, which is often used to remove noise associated with differentiations and ensure the entire feedback controller $H(s)N(s)$ is proper in practical applications.

The coefficients of the CLTF in Equation (13) varies with wave frequency. Therefore, stability and control bandwidth of PI _{b} D _{a} controller with various combinations of a and b are studied when the controller is tuned at four typical wave frequencies, respectively. At each wave frequency, the CLTF becomes a transfer function with constant coefficients consisting of hydrodynamic coefficients at that frequency for typical frequency-domain analysis (e.g. pole-zero map and Bode diagram).

4.2 | Stability analysis

In order to understand the stability of the WEC system under PI _{b} D _{a} control (and its transition from PI control to PD control), the pole locations of the CLTF in Equation (13) given A^ω , B_{rad}^ω , and B_{vd}^ω at $\omega = 0.9$ rad/s ($T_\omega = 7$ s) and five combinations of a and b are shown in Figure 3. It is evident that when b decreases from 1 to 0 (and a increases from 0 to 1), during which PI control changes to PD control, the CLTF poles move from a lightly damped stable location (blue cross in Figure 3) towards a heavily damped marginally stable location (dark red

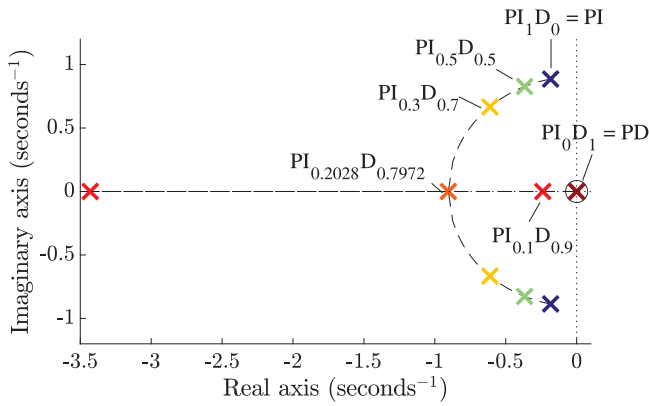


FIGURE 3 Pole locations of the closed-loop WEC system under PID control (tuned for $\omega = 0.9$ rad/s) with five ratios of Integral and Derivative components (PI_bD_a). The trajectories in dashed lines show how pole locations change with the decrease of b and increase of a

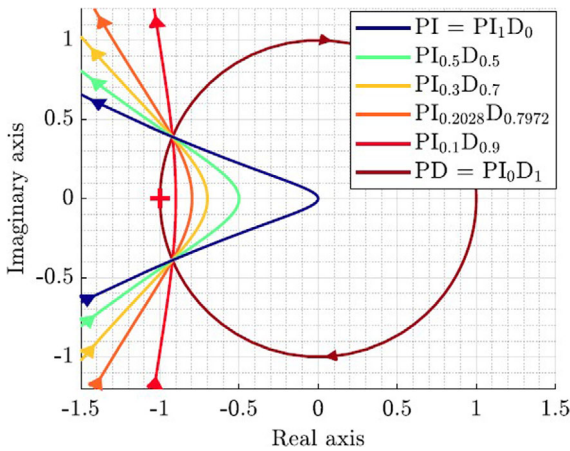


FIGURE 4 Nyquist plot showing stability margins of the closed-loop WEC system under PID control (tuned for $\omega = 0.9$ rad/s) with five ratios of Integral and Derivative components (PI_bD_a). The Nyquist contour under PD control (in scarlet) and the unit circle overlap each other. The red cross mark highlights the critical point $[-1 \ 0]$

cross in Figure 3) and asymptotically becoming marginally stable. With a decrease in b (and an increase in a), the transition of the pole locations is slow towards the critical point (orange cross in Figure 3 associated with $PI_{0.2028}D_{0.7972}$), followed by a rapid transition towards the marginally stable location when b further decreases towards 0 (during which spring control vanishes). Furthermore, following Routh–Hurwitz stability criterion, the closed-loop system is found to be always stable when $0 \leq a < 1$ and $a + b = 1$ (the requirement for satisfying resonance conditions).

The CLTF pole locations indicate that the stability margins of the closed-loop system need further investigations, and thus the Nyquist plot of $G(s)H(s)$ is shown in Figure 4. It can be found that the phase margins are the same, 23 degrees (or 0.44 s), for all the PI_bD_a controller candidates, whilst the gain margin decreases from infinity for PI control to 1 for PD control with an increase in a . The gain margin of $PI_{0.2028}D_{0.7972}$ controller is 1.25, which implies that the closed-loop system can still be sta-

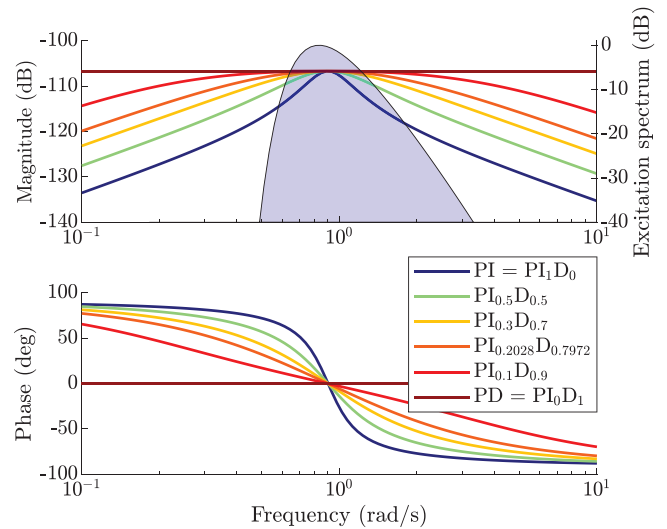


FIGURE 5 Bode diagram showing the frequency response of the closed-loop WEC system under PID control (tuned for $\omega = 0.9$ rad/s) with five ratios of Integral and Derivative components (PI_bD_a). Upper and lower plots show respectively the magnitude and phase relationship between $F_{exc}(s)$ and $\dot{z}(s)$

ble subjected to 25% error in the gain of the open-loop transfer function. The results of CLTF pole locations and stability margins show that PI control is more stable and robust than PD control and thus PI_bD_a control with $b < 0.2$ and $a > 0.8$ should be avoided from the control stability perspective.

4.3 | Control bandwidth analysis

In order to understand the control bandwidth of the WEC system under PI_bD_a control when the controller is tuned at a single wave frequency, 0.9 rad/s in this case, the hydrodynamic coefficients in the CLTF in Equation (13) are fixed at $\omega = 0.9$ rad/s, and the broadband frequency response of the CLTF is shown in Figure 5. It is evident that with an increase in the Derivative/mass control component (and a corresponding decrease in the Integral/spring control component) in PID control, the magnitude response of the buoy velocity increases across the wave frequency range towards the response at resonance (0.9 rad/s) as shown in the upper magnitude plot, while the phase of the buoy velocity converges towards the phase of the excitation force across the wave frequency range as shown in the lower phase plot. Therefore, an increase in Derivative/mass control component (a) in PI_bD_a control increases the control bandwidth of the WEC system. In extreme cases, the WEC system operates optimally only at the resonance frequency under PI control, whilst operates at near-optimal across the wave frequencies under PD control. In practice when excited by irregular waves, the WEC system will respond to a wide range of input (excitation force) frequencies as illustrated by a PM spectrum with $T_c = 7$ s and $H_s = 2$ m (shaded region) as shown in the magnitude plot of Figure 5. Therefore, control bandwidth plays a key role in maximising the power absorption bandwidth

of WEC in irregular waves when the controller is pre-tuned at optimal for one dominant wave period only (e.g. T_c) and fixed during operation.

CLTF stability and control bandwidth are also studied when the controller is tuned at 0.48, 0.57 and 0.7 rad/s respectively, which demonstrate trends consistent with the results at 0.9 rad/s. Therefore, $PI_{0.2}D_{0.8}$ is a close-to-optimal configuration regardless of wave frequency from the stability and control bandwidth perspective, and thus is selected as a candidate for time-domain analysis.

5 | POWER PERFORMANCE ANALYSIS IN TIME DOMAIN

5.1 | Simulation setup

5.1.1 | General settings

To further analyse the power performance of the proposed controllers, a time-domain model following Equation (2) is assembled in MATLAB/Simulink setting the fixed time step of 0.01 s and the solver as automatic.

The average power absorbed by the WEC is calculated as:

$$\bar{P}_{\text{total}} = -\frac{1}{T} \int_0^T F_{\text{pto}}(t) \dot{\zeta}(t) dt, \quad (14)$$

and only for PP²ID control, the total power can be decomposed into the power absorbed by the linear damper (P term) and by the quadratic damper (P² term) respectively:

$$\bar{P}_P = \frac{1}{T} \int_0^T (B_{\text{pto}} \cdot \dot{\zeta}(t)) \dot{\zeta}(t) dt, \quad (15)$$

$$\bar{P}_{P^2} = \frac{1}{T} \int_0^T (\rho C_D A_D |\dot{\zeta}(t)| \dot{\zeta}(t)) \dot{\zeta}(t) dt, \quad (16)$$

where F_{pto} and $\dot{\zeta}$ are the instantaneous PTO force and buoy velocity respectively. To remove the transient dynamic response, only the last 20 cycles (out of the total 100 simulated cycles) are used to calculate the average power output in the regular wave simulations, and the last 300 cycles (out of the total 400 simulated cycles) are used for average power calculation in the irregular wave simulations. Typical wave periods from 6 to 13 s with an increment of 1 s are used in the simulations, so the corresponding wave frequencies ranges from 0.48 to 1.05 rad/s. The wave height is set to 2 m unless otherwise stated.

5.1.2 | PTO parameter tuning

To provide a fair comparison of the control strategies, control parameters are optimised according to the procedure below.

Regular wave analysis

PID: $B_{\text{rad}}^\omega + B_{\text{vd}}^\omega$ are found via grid search [30]; the spring control coefficient is estimated by $\omega^2(m + \mathcal{A}^\omega)$ and scaled by a pre-defined value of b ; and the mass control coefficient ($m + \mathcal{A}^\omega$) is scaled by a pre-defined value of a , as shown in Equation (11) to achieve PI_bD_a control.

PP²ID: Due to the separation of control forces associated with radiation damping term and viscous drag term, all the control coefficients can be obtained analytically without offline optimisation, following Equation (12) given predefined a and b .

The maximum power absorbed by the PID and PP²ID controllers with frequency-dependent optimal PTO parameters in regular waves are labelled as PID-max, and PP²ID-max respectively. When the controllers use fixed PTO parameters only optimal for a single wave period (e.g. 7 s), results will be labelled as PID-7s and PP²ID-7s respectively.

Irregular wave analysis

In this work, irregular waves are modelled using the Pierson–Moskowitz (PM) spectrum [31]. The relation between energy period T_c and peak period T_p for the PM spectrum is [31]: $T_c = 0.858T_p$. There are two methods to achieve optimisation for the proposed controllers in irregular waves. The first method is to do a brute-force optimisation based on the entire PM spectrum to obtain the optimal PTO parameters in irregular waves, with predefined a and b . The maximum power resulting from the optimal PTO parameters is denoted as PID-S and PP²ID-S respectively. The second method uses the optimal PTO parameters obtained for a regular wave with a wave period of T_c to estimate the optimal PTO parameters described by the PM spectrum (T_p) in irregular waves, which is denoted as PID- T_c and PP²ID- T_c respectively. Thus, in the second method, close-to-optimal PTO parameters can be determined analytically for PP²ID control, which is attractive for practical applications. The first method, on the other hand, is computationally expensive and thus is only used to benchmark the performance of the second method in this study.

5.2 | Power analysis under regular wave conditions

5.2.1 | Proportional, integral and derivative (PID) control

It has been shown in Section 3 that in theory the frequency-dependent resonance condition can be satisfied under PI_bD_a control when $a + b = 1$, which, together with attaining optimal amplitude condition (also frequency-dependent), leads to maximum power absorption of WEC in regular waves. This theory is further validated using a time-domain simulation, with results shown in Figure 6, where maximum power absorption of the WEC under PI_bD_a control with four sets of b and a combinations (denoted as PI_bD_a -max) are plotted against typical wave frequencies. It is evident that the three PI_bD_a controllers with $a + b = 1$ have identical maximum power absorption across the

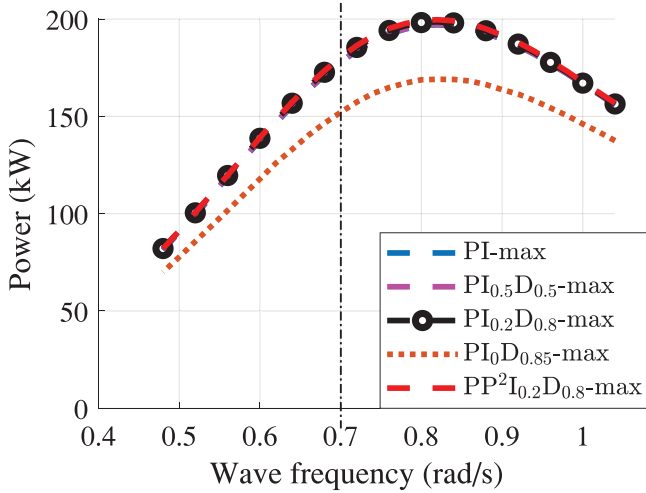


FIGURE 6 Maximum power absorption of $PI_b D_a$ controllers and $PP^2 I_{0.2} D_{0.8}$ controller in regular wave condition, against typical wave frequencies and at 2 m wave height. The corresponding time series data of PTO forces at $\omega = 0.7$ rad/s (highlighted by the vertical dashed-dotted line) are shown in Figure 7

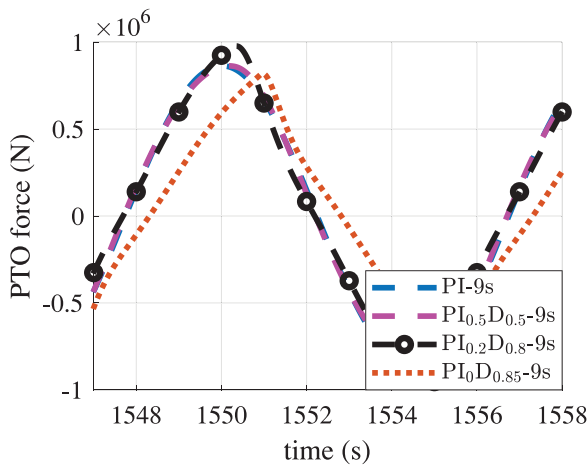


FIGURE 7 Time series data of PTO force in regular wave of 9 s wave period ($\omega = 0.7$ rad/s) under $PI_b D_a-9s$ control

entire wave frequency range. Compared to other three controllers, $PI_0 D_{0.85}$ -max is about 14% less efficient across the entire wave frequency range, because the resonance condition is not satisfied. The curve of $PP^2 I_{0.2} D_{0.8}$ -max will be discussed in next section. The corresponding time series data of PTO forces at $\omega = 0.7$ rad/s under $PI_b D_a-9s$ control are shown in Figure 7. It is evident that the phase and magnitude of the PTO force under $PI_0 D_{0.85}$ control is degraded compared to other three controllers who show almost identical PTO force pattern. With an increase in a , the PTO force starts to show nonlinear behaviour near the peaks, which indicates that the derivative/mass control component is sensitive to time delay in the feedback.

In practice due to model uncertainty, unknown disturbances and the sub-optimal nature of causal control in stochastic waves, PID control is not always tuned at its optimal conditions for

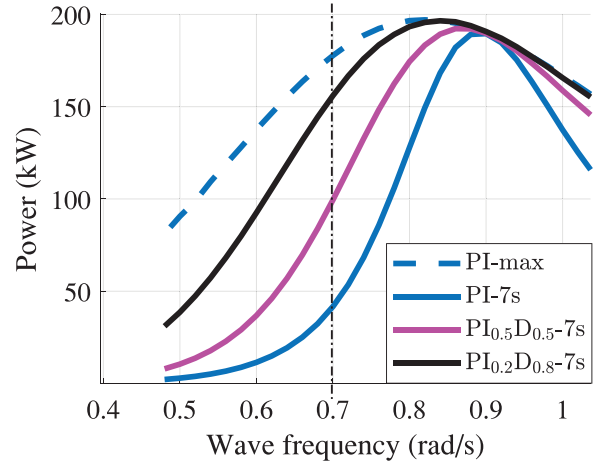


FIGURE 8 Power absorption bandwidth of $PI_b D_a$ control tuned at optimal for 7 s wave period ($\omega = 0.9$ rad/s) ($PI_b D_a-7s$, solid lines), and maximum power absorption of PI control at each wave period (PI-max, blue dashed line). The corresponding time series data of buoy velocities at $\omega = 0.7$ rad/s (highlighted by the vertical dashed-dotted line) are shown in Figure 9

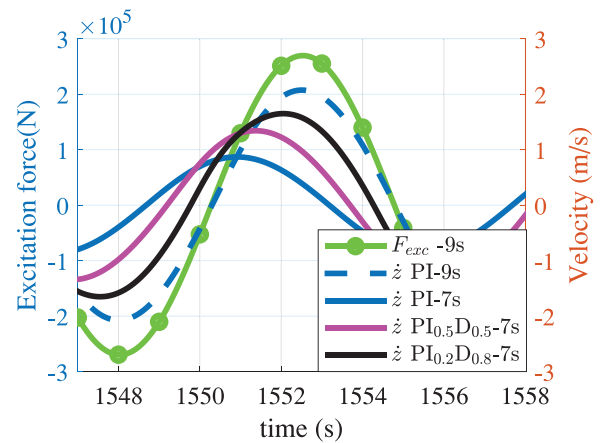


FIGURE 9 Time series data of excitation force (green circled line) in regular wave of 9 s wave period ($\omega = 0.7$ rad/s) and corresponding buoy velocities under $PI_b D_a-7s$ control (solid lines) and under PI-9s control (blue dashed line)

power absorption. Therefore, the power bandwidth of PID control near its tuned optimal condition (e.g. resonance) is investigated, with results shown in Figure 8, where power absorption of the WEC under $PI_b D_a$ control tuned for 7 s wave period ($\omega = 0.9$ rad/s) (expressed as $PI_b D_a-7s$) are plotted against typical wave frequencies. The blue dashed curve shows the maximum power absorption of PI control at each wave frequency extracted from Figure 6 for a comparison. It is evident that the power bandwidth of $PI_{0.2} D_{0.8}-7s$ is widest among the tested $PI_b D_a-7s$ categories and is close to that of PI-max control. These results can be explained by the control bandwidth diagram in Figure 5 and the time series plot in Figure 9. It is evident in both figures that at resonance where control is tuned at optimal for the incident wave, the buoy velocity is in phase with the excitation force. On the other hand, at

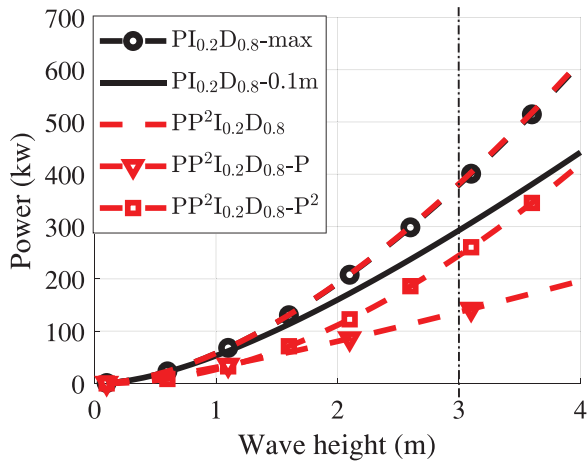


FIGURE 10 Power absorption performance of $PI_{0.2}D_{0.8}$ control tuned at optimal for each wave height ($PI_{0.2}D_{0.8}$ -max) and for 0.1 m wave height ($PI_{0.2}D_{0.8}$ -0.1m), and power absorption performance of $PP^2I_{0.2}D_{0.8}$ control optimal regardless of wave heights, against typical wave heights and at 7 s wave period. The triangle-dashed line and the square-dashed line represent the power absorbed by the linear damper and quadratic damper respectively under $PP^2I_{0.2}D_{0.8}$ control. The corresponding time series data of PTO forces and buoy displacement/velocity response at 3 m wave height (highlighted by the vertical dashed-dotted line) are shown in Figures 11 and 12 respectively

off-resonance where control is not optimally tuned for the incident wave, with a decrease in the ratio of D term in PID control, the phase lag in the buoy velocity increases, whilst the magnitude of the buoy velocity decreases, leading to less and less power absorption.

5.2.2 | Proportional, integral, derivative and drag (PP^2ID) control

PP^2ID control is proposed on top of PID control, aiming to analytically determine the optimal control force without time-consuming linearisation of the viscous drag term or brute-force search. Therefore, when tuned optimally in regular waves, PP^2ID control and PID control show identical maximum power absorption performance as shown in Figure 6.

In addition, since no longer reliant on wave-dependent optimisation, PP^2ID control is more robust than PID control when the incident wave height changes, as shown in Figure 10. It is evident that $PP^2I_{0.2}D_{0.8}$ control absorbs an identical amount of power as optimally tuned $PI_{0.2}D_{0.8}$ control with wave height-dependent PTO parameters (denoted as $PI_{0.2}D_{0.8}$ -max), and absorbs increasingly more power than $PI_{0.2}D_{0.8}$ control with fixed PTO parameters tuned for 0.1 m wave height (denoted as $PI_{0.2}D_{0.8}$ -0.1m) with an increase in the wave height. At 4 m wave height, $PP^2I_{0.2}D_{0.8}$ control absorbs 30% more power than $PI_{0.2}D_{0.8}$ -0.1m control. The total power absorbed under $PP^2I_{0.2}D_{0.8}$ control is divided into the power absorbed by the linear damper (triangle-dashed line) and by the quadratic damper (square-dashed line) respectively. It can be seen that with an increase in wave height, the quadratic damper absorbed power becomes more and more dominant compared to the lin-

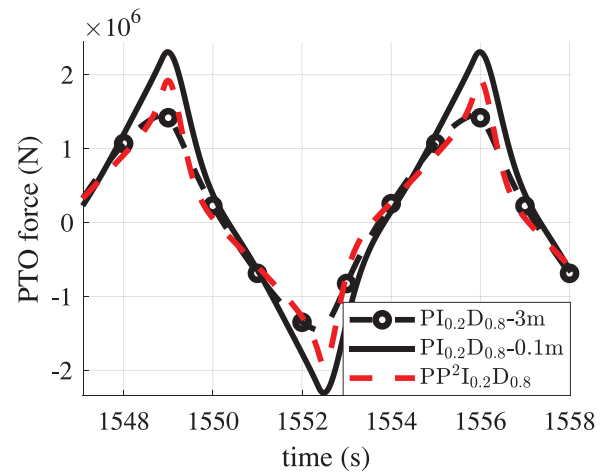


FIGURE 11 Time series data of PTO force at 7 s wave period and 3 m wave height under $PI_{0.2}D_{0.8}$ control and $PP^2I_{0.2}D_{0.8}$ control respectively

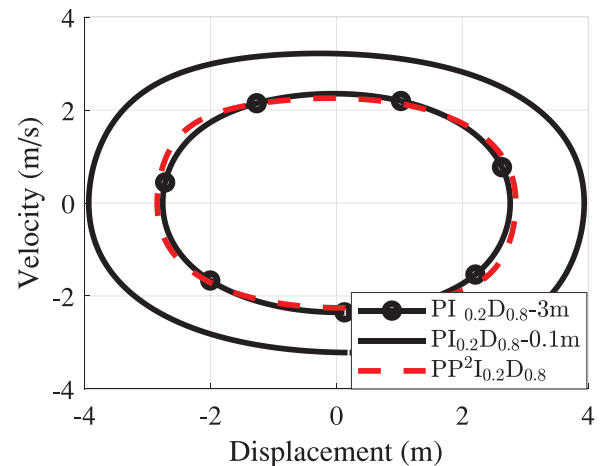


FIGURE 12 Time series data of buoy displacement-velocity response at a wave period of 7 s and a wave height of 3 m under $PI_{0.2}D_{0.8}$ control and $PP^2I_{0.2}D_{0.8}$ control respectively

ear damper absorbed power. The corresponding time series data of PTO forces at 7 s wave period and 3 m wave height under $PI_{0.2}D_{0.8}$ control and $PP^2I_{0.2}D_{0.8}$ control are shown in Figure 11. It is evident that when sub-optimally tuned (e.g. comparing $PI_{0.2}D_{0.8}$ -0.1m and $PI_{0.2}D_{0.8}$ -3m), $PI_{0.2}D_{0.8}$ control can overestimate the PTO force by more than 50% at peaks. $PP^2I_{0.2}D_{0.8}$ control, on the other hand, generates about 25% more PTO force at peaks than optimally tuned $PI_{0.2}D_{0.8}$ control ($PI_{0.2}D_{0.8}$ -3m) does. The corresponding buoy velocity-displacement plot at a wave period of 7 s and a wave height of 3 m is shown in Figure 12. It is evident that $PP^2I_{0.2}D_{0.8}$ control results in almost identical displacement/velocity response compared to the optimally tuned $PI_{0.2}D_{0.8}$ control ($PI_{0.2}D_{0.8}$ -3m), whilst suboptimally tuned $PI_{0.2}D_{0.8}$ control ($PI_{0.2}D_{0.8}$ -0.1m) leads to about 30% higher displacement/velocity response.

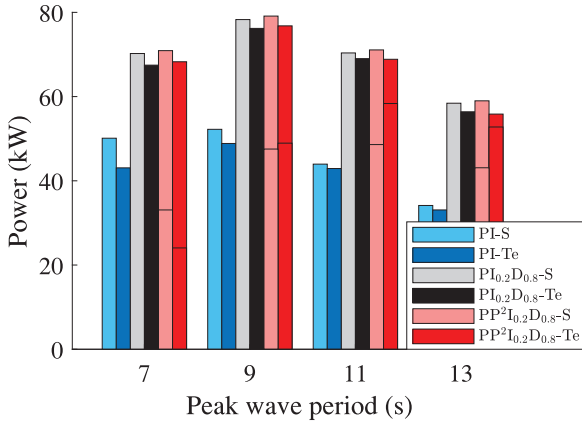


FIGURE 13 A comparison of power performance of PI, $PI_{0.2}D_{0.8}$ and $PP^2I_{0.2}D_{0.8}$ controllers in irregular waves against peak wave periods of the irregular wave spectrum, where -Te denotes that the optimal PTO parameters of the controller in regular wave at T_e wave period are used and -S denotes that the actual optimal PTO parameters for the irregular wave spectrum are used in simulation. The horizontal bar divides the total power absorbed under $PP^2I_{0.2}D_{0.8}$ into the linear damper absorbed power (upper section) and the quadratic damper absorbed power (lower section)

5.3 | Power analysis under irregular wave conditions

The proposed causal controllers are sub-optimal in irregular wave conditions, which are investigated using time-domain simulations in this subsection. The power absorption of PI, $PI_{0.2}D_{0.8}$ and $PP^2I_{0.2}D_{0.8}$ controllers in irregular waves using the optimal PTO parameters obtained under a regular wave with a wave period T_e , denoted as PI-Te, $PI_{0.2}D_{0.8}$ -Te and $PP^2I_{0.2}D_{0.8}$ -Te respectively, are shown in Figure 13, as well as the power absorption of these controllers using the actual optimal PTO parameters for the irregular wave spectrum, denoted as PI-S, $PI_{0.2}D_{0.8}$ -S and $PP^2I_{0.2}D_{0.8}$ -S for a comparison. It is evident that the on average the power absorbed by the PI control with estimated PTO parameters (PI-Te) is 6.5% lower than the maximum power absorbed by PI control (PI-S) across the tested irregular wave conditions. For the $PI_{0.2}D_{0.8}$ control and $PP^2I_{0.2}D_{0.8}$ control respectively, on average the power absorption using the estimated PTO parameters ($PI_{0.2}D_{0.8}$ -Te and $PP^2I_{0.2}D_{0.8}$ -Te) is only 3% less than the power absorption using the actual optimal PTO parameters determined from brute-force optimisation ($PI_{0.2}D_{0.8}$ -S and $PP^2I_{0.2}D_{0.8}$ -S). The power absorbed by $PI_{0.2}D_{0.8}$ control with estimated PTO parameters is in average 21.8% (with a standard deviation of 6.2%) higher than the maximum power absorbed by PI control. $PP^2I_{0.2}D_{0.8}$ shows almost identical power absorption performance to $PI_{0.2}D_{0.8}$. These results can be explained by the findings on the power absorption bandwidth of the controllers from regular wave analysis. The derivative/mass control term plays a key role in both the PID and PP^2ID controllers that functions to widen the power absorption bandwidth of the controller and thus makes WEC power absorption more effective across a broad range of wave frequencies near the energy period of the irregular wave spectrum. This is expected since the D term acts

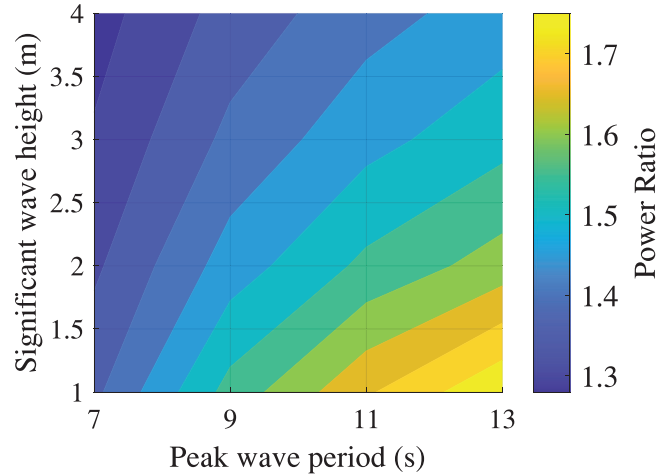


FIGURE 14 Power absorption ratio of ($PP^2I_{0.2}D_{0.8}$ -Te/PI-S) in irregular waves across grids of sea states. Both controllers use optimal PTO settings for each sea state

to reduce the mass reactance, thereby leaving only the intrinsic resistance of the buoy which is matched to the resistance of the fluid.

The maximum power absorption performance of PP^2ID controller is further investigated in irregular wave simulations across a grid of sea states in comparison to that of standard PI control, with results shown in Figure 14, where the power absorption ratio of $PP^2I_{0.2}D_{0.8}$ -Te control over PI-S control is plotted against significant wave heights and peak wave periods. It is evident that $PP^2I_{0.2}D_{0.8}$ -Te control absorbs in average 50% more power than PI-S control across all the tested sea states. With an increase in the peak wave period and a decrease in the significant wave height, the power ratio increases from 1.27 (at $T_p = 7$ s and $H_s = 4$ m) to 1.74 (at $T_p = 13$ s and $H_s = 1$ m).

To achieve maximum power absorption of PP^2ID control and PI control at each single sea state, it is necessary to adapt the PTO parameters to the current sea state that varies on an hourly basis and thus is difficult to implement in practice. Therefore, PP^2ID control and PI control using the fixed optimal control parameters for the sea state of $T_p = 7$ s and $H_s = 2$ m are tested and compared across grids of sea states, with results shown in Figure 15. The power absorption ratio of $PP^2I_{0.2}D_{0.8}$ -Te_{7s&2m} over PI-Te_{7s&2m} ranges between 1.56 and 3.76, resulting in a mean power ratio of 2.5 with a standard deviation of 0.83 across all the tested sea states. This indicates that $PP^2I_{0.2}D_{0.8}$ control is in average 2.5 times more efficient than standard PI control when their PTO parameters are pre-tuned at optimal for a single/dominant sea state.

6 | CONCLUSION

This paper studied the power performance of the causal PID and PP^2ID feedback controllers, as inspired by Phi method, against that of PI control, on a fully submerged heaving point absorber WEC under both regular and irregular wave conditions. The study was conducted based on the well-known linear

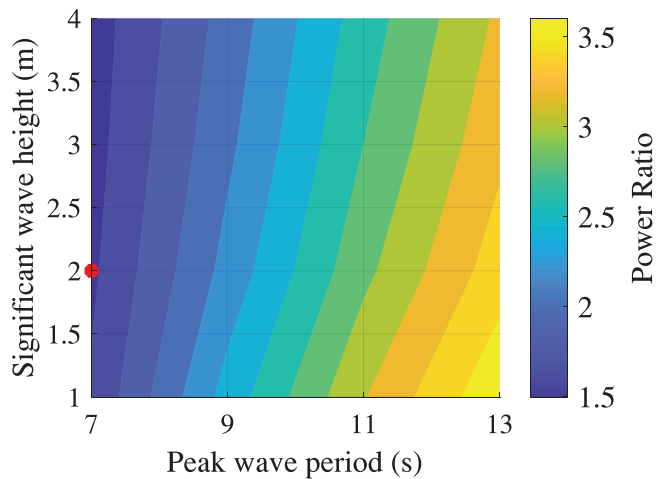


FIGURE 15 Power absorption ratio of (PP²I_{0.2}D_{0.8}-Te_{7s&2m}/PI-Te_{7s&2m}) in irregular waves across grids of sea states. Both controllers use fixed optimal PTO setting for $T_p = 7$ s and $H_s = 2$ m (labelled as a red asterisk)

wave theory model assuming small waves and WEC motions, which presents a major limitation for the work. The requirements for practical implementation of PID control is considered as common knowledge [32] and thus was not explicitly discussed in the paper (e.g. low-pass filters, requirement for the controller to be proper, and other common PID modifications such as anti-windup control).

The WEC system under PID control (when $0 \leq a \leq 1$ and $a + b = 1$) is stable according to frequency-domain analysis except for PI₀D₁ (pure PD control), which is marginally stable, however, the portion of Derivative component in PID control needs to be restricted to provide sufficient stability margins considering model uncertainties. PD control has wider control bandwidth than PI control for the fully submerged case considered in this paper. PI_{0.2}D_{0.8} is a close-to-optimal configuration considering trade-off between stability and control bandwidth. The frequency-domain analysis conducted in this paper did not consider system internal-stability and sensitivity, which will be considered in future work.

Time-domain simulations show that the maximum power absorption performance of PI and PI_{0.2}D_{0.8} controls in regular wave condition are similar. However, the power bandwidth of PID (across wave frequencies) is wider than that of PI, which results in that the maximum absorbed power of PI_{0.2}D_{0.8} is on average 22% higher than that of PI control in irregular wave conditions of $H_s = 2$ m and $T_p = 7$ –13 s. However, the D term component in PID control is sensitive to the time delay in the feedback, which induces nonlinear behaviour in the PTO force profile.

PP²ID control, as a combination of PID control and quadratic damper control, demonstrates its advantages in both power absorption bandwidth (across wave heights) and PTO tuning efficiency over PID control. PP²I_{0.2}D_{0.8} control (whose PTO parameters are determined fully analytically) can achieve similar maximum power absorption of optimal PI_{0.2}D_{0.8} control (whose PTO parameters are determined via wave-condition dependent optimisation) in both regular and irregular waves.


PP²I_{0.2}D_{0.8} control generates more PTO force than PI_{0.2}D_{0.8} control (when optimally tuned) does, however, generates less PTO force than PI_{0.2}D_{0.8} control (when sub-optimally tuned) does. PP²I_{0.2}D_{0.8} control generates almost identical displacement/velocity response as the optimally tuned PI_{0.2}D_{0.8} control but less displacement/velocity response than suboptimally tuned PI_{0.2}D_{0.8} control. PP²I_{0.2}D_{0.8} control with fixed PTO parameters (optimal for a single sea state only) is in average 2.5 times more efficient than PI control with fixed PTO parameters when both controllers operate across sea states of $T_p = 7$ –13 s and $H_s = 1$ –4 m without the consideration on sea state probability. Despite its high tuning efficiency and strong robustness against changes in wave height and frequency, PP²I_{0.2}D_{0.8} control is not capable of handling constraints, like most impedance matching control strategies.

Future work will focus on investigating the robustness and performance of the PID and PP²ID controllers in real WEC applications subjected to model uncertainties and disturbances in the hydrodynamics, by using nonlinear hydrodynamic model (e.g. Weak Scatter model [24]) instead of linear wave theory based model. Furthermore, the impact of time delay and higher order dynamics in the sensor measurements on the performance of the proposed feedback controllers will also be studied. Attempts will also be made to compare the proposed controller with other optimisation-based controllers that are capable of accommodating nonlinear dynamics and constraints such as dynamic programming.

ORCID

Yifeng Gu  <https://orcid.org/0000-0001-6157-1008>

Boyin Ding  <https://orcid.org/0000-0001-8417-8057>

Natalia Y. Sergienko  <https://orcid.org/0000-0002-3418-398X>

REFERENCES

1. Cruz, J.: Ocean wave energy: Current status and future perspectives. Green Energy and Technology, Springer, Berlin, Heidelberg (2008)
2. Ringwood, J.V., et al.: Energy-maximizing control of wave-energy converters: the development of control system technology to optimize their operation. *Control Syst.*, IEEE 34(5), 30–55 (2014)
3. Falnes, J.: Ocean waves and oscillating systems: Linear interactions including wave-energy extraction. *Appl. Mech. Rev.* 56(1), B3 (2003)
4. Garcia Violini, D., et al.: Simple controllers for wave energy devices compared. *J. Mar. Sci. Eng.* 8(10), 793 (2020)
5. Falnes, J.: On non-causal impulse response functions related to propagating water waves. *Appl. Ocean Res.* 17(6), 379–389 (1995)
6. Hals, J., Falnes, J., Moan, T.: Constrained optimal control of a heaving buoy wave-energy converter. *J. Offshore Mech. Arct. Eng.* 133(1), 011401 (2011)
7. Fusco, F., Ringwood, J.V.: Short-term wave forecasting for real-time control of wave energy converters. *IEEE Trans. sustainable energy* 1(2), 99–106 (2010)
8. Tona, P., Sabiron, G., Nguyen, H.N.: An energy-maximising MPC solution to the WEC control competition. In: *International Conference on Offshore Mechanics and Arctic Engineering*, vol. 58899. American Society of Mechanical Engineers, New York (2019)
9. Coe, R.G., Bacelli, G., Forbush, D.: A practical approach to wave energy modeling and control. *Renewable Sustainable Energy Rev.* 142, 110791 (2021)

10. Babarit, A., et al.: Numerical benchmarking study of a selection of wave energy converters. *Renewable Energy* 41, 44–63 (2012)
11. Coe, R., et al.: MASK3 for advanced WEC dynamics and controls. (Marine and Hydrokinetic Data Repository (MHKDR), Sandia National Laboratories, Carlsbad, NM (2019))
12. Abdelkhalik, O., et al.: Multiresonant feedback control of a three-degree-of-freedom wave energy converter. *IEEE Trans. Sustainable Energy* 8(4), 1518–1527 (2017)
13. Coe, R.G., et al.: A comparison of control strategies for wave energy converters. *Int. J. Mar. Energy* 20, 45–63 (2017)
14. Ringwood, J.V., et al.: An analytical and numerical sensitivity and robustness analysis of wave energy control systems. *IEEE Trans. Control Syst. Technol.* 28(4), 1337–1348 (2019)
15. Penalba, M., Giorgi, G., Ringwood, J.V.: Mathematical modelling of wave energy converters: A review of nonlinear approaches. *Renewable Sustainable Energy Rev.* 78, 1188–1207 (2017)
16. Sergiienko, N.Y., et al.: Feasibility study of the three-tether axisymmetric wave energy converter. *Ocean Eng.* 150, 221–233 (2018)
17. Zou, S., et al.: Optimal control of wave energy converters. *Renewable energy* 103, 217–225 (2017)
18. Mills, B., Ding, B.: Improving wave-absorber power. In: Lewis, A. (ed.) 12th European Wave and Tidal Energy Conference Series, (EWTEC), pp. 1119-1–1119-6. University of Adelaide, Adelaide (2017)
19. Morison, J., Johnson, J., Schaaf, S.: The force exerted by surface waves on piles. *J. Pet. Technol.* 2(05), 149–154 (1950)
20. Cummins, W.E.: The impulse response function and ship motions. David Taylor Model Basin Reports, MIT Press, Cambridge, MA (1962)
21. Perez, T., Fossen, T.I.: A Matlab toolbox for parametric identification of radiation-force models of ships and offshore structures. *Modeling, Identification Control* 30(1), 1–15 (2009)
22. Linton, C.M.: Radiation and diffraction of water waves by a submerged sphere in finite depth. *Ocean Eng.* 18(1-2), 61–74 (1991)
23. Hoerner, S.F.: Fluid-dynamic drag: practical information on aerodynamic drag and hydrodynamic resistance. Hoerner Fluid Dynamics, Cambridge University Press, Cambridge (1965)
24. Ding, B., et al.: Comparison of wave-body interaction modelling methods for the study of reactively controlled point absorber wave energy converter. Paper presented at 34th International Workshop on Water Waves and Floating Bodies (IWWWF), Newcastle, 7–10 April 2019
25. Hals, J., Falnes, J., Moan, T.: A comparison of selected strategies for adaptive control of wave energy converters. *J. Offshore Mech. Arct. Eng.* 133(3), 031101–031101 (2011)
26. Hansen, R.: Design and control of the power take-off system for a wave energy converter with multiple absorbers. Ph.D. Thesis, Aalborg University (2013)
27. Terra, G.M., van de Berg, W.J., Maas, L.R.: Experimental verification of lorentz-linearization procedure for quadratic friction. *Fluid Dyn. Res.* 36(3), 175 (2005)
28. Folley, M., Whittaker, T., Van't Hoff, J.: The design of small seabed-mounted bottom-hinged wave energy converters. In: Proceedings of the 7th European Wave and Tidal Energy Conference, pp. 1–10. Queen's University, Belfast (2007)
29. Bacelli, G., Ringwood, J.: Constrained control of arrays of wave energy devices. *Int. J. Mar. Energy* 2013(3), e53–e69 (2013)
30. Gu, Y., Ding, B., Sergiienko, N.Y.: Power maximising control of heaving point absorber wave energy converters using quadratic damping force. Paper presented at The Fourteenth ISOPE Pacific/Asia Offshore Mechanics Symposium, Dalian. (International Society of Offshore and Polar Engineers, Dalian, 22 November 2020)
31. The Specialist Committee on Waves. Final report and recommendations to the 23rd ITTC. In: Proceedings of the 23rd International Towing Tank Conference. vol. II, pp. 505–736. ITTC, Zürich (2002)
32. Åström, K.J., Hägglund, T., Astrom, K.J.: Advanced PID control, vol. 461. ISA-The Instrumentation, Systems, and Automation Society Research, Triangle Park (2006)

How to cite this article: Gu Y, Ding B, Sergiienko NY, Cazzolato BS. Power maximising control of a heaving point absorber wave energy converter. *IET Renew. Power Gener.* 2021;15:3296–3308. <https://doi.org/10.1049/rpg2.12252>

APPENDIX A: DERIVATION PROCEDURES FOR THE OPTIMAL CONTROL FORCE USING PHI METHOD

This section shows how to use Phi method to derive the optimal control force F_{pto} based on the analytical expressions of the system dynamics (H) as shown in Table 2, where the spring term and the viscous drag term are used as two typical examples here.

A.1 | Spring

Substituting $H = a_0 \zeta(t)$ into Equation (4), we have:

$$F_{pto}(t) = \int_0^t \dot{\zeta} \frac{\partial}{\partial \zeta} a_0 \zeta(\tau) d\tau - \sum_{k=1}^{\infty} \left(-\frac{\partial}{\partial t} \right)^{k-1} \left(\dot{\zeta} \frac{\partial}{\partial \zeta^{(k)}} a_0 \zeta(t) \right). \quad (A.1)$$

The sum term in Equation (A1) disappears since partial derivative of $H = a_0 \zeta(t)$ with respect to $\zeta^{(k)}$ (when $k \geq 1$) is always zero. Thus, solving the integral term leads to:

$$F_{pto}(t) = \int_0^t \dot{\zeta} \frac{\partial}{\partial \zeta} a_0 \zeta(\tau) d\tau = a_0 \zeta(t). \quad (A.2)$$

A.2 | Viscous drag

As for the viscous drag term $H = a_3 |\dot{\zeta}(t)| \dot{\zeta}(t)$, it can be alternatively written as $H = a_3 \operatorname{sgn}(\dot{\zeta}) (\dot{\zeta})^2$. Substituting it into Equation (4), we have:

$$\begin{aligned} F_{pto}(t) &= \int_0^{f(\dot{\zeta}>0)} \dot{\zeta} \frac{\partial}{\partial \zeta} a_3 (\dot{\zeta})^2 d\tau - \int_0^{f(\dot{\zeta}<0)} \dot{\zeta} \frac{\partial}{\partial \zeta} a_3 (\dot{\zeta})^2 d\tau \\ &\quad - a_3 \operatorname{sgn}(\dot{\zeta}) \sum_{k=1}^{\infty} \left(-\frac{\partial}{\partial t} \right)^{k-1} \left(\dot{\zeta} \frac{\partial}{\partial \zeta^{(k)}} (\dot{\zeta})^2 \right) = \\ &= -a_3 \operatorname{sgn}(\dot{\zeta}) \left(\dot{\zeta} \frac{\partial (\dot{\zeta})^2}{\partial \zeta} \right) = -2a_3 \operatorname{sgn}(\dot{\zeta}) (\dot{\zeta})^2 = -2a_3 |\dot{\zeta}(t)| \dot{\zeta}(t). \end{aligned} \quad (A.3)$$

APPENDIX B: MATHEMATICAL PROOF ON TRIPLING VISCOUS DRAG FOR MAXIMUM POWER ABSORPTION

To simply the proof, it is assumed that the reactance terms in the WEC dynamics (e.g. mass and spring) are cancelled by the control force following impedance matching theory and the radiation effect is ignored. Then the WEC dynamics in Equation (2)

can be written as:

$$a_3|\dot{\chi}(t)|\dot{\chi}(t) = F_{\text{exc}}(t) + F_{\text{pto}}(t). \quad (\text{B.1})$$

Assuming $F_{\text{pto}}(t)$ in Equation (B1) is a quadratic damper control force, $F_{\text{pto}}(t) = -\alpha a_3|\dot{\chi}(t)|\dot{\chi}(t)$ where α is unknown, and combining common terms, Equation (B1) becomes:

$$|\dot{\chi}(t)|\dot{\chi}(t) = F_{\text{exc}}(t)/(a_3 + \alpha a_3). \quad (\text{B.2})$$

The average power absorbed by the PTO, or more specifically by the quadratic damper in the PTO is given by:

$$\bar{P} = -\frac{1}{T} \int_0^T F_{\text{pto}}(t)\dot{\chi}(t)dt = \frac{1}{T} \int_0^T \alpha a_3|\dot{\chi}(t)|\dot{\chi}(t)^2 dt, \quad (\text{B.3})$$

where T is the sampling period for average. Substituting Equation (B2) into Equation (B3) gives:

$$\bar{P} = \frac{1}{T} \int_0^T \alpha a_3 \left(\frac{|F_{\text{exc}}(t)|}{a_3 + \alpha a_3} \right)^{\frac{3}{2}} dt$$

$$dt = \frac{1}{T} \int_0^T \frac{\alpha}{(1 + \alpha)^{\frac{3}{2}}} a_3^{-\frac{1}{2}} |F_{\text{exc}}(t)|^{\frac{3}{2}} dt. \quad (\text{B.4})$$

Solving $\partial \bar{P} / \partial \alpha = 0$, maximum power absorption occurs when $\alpha = 2$, which follows the Phi-derived control force $F_{\text{pto}}(t) = -2a_3|\dot{\chi}(t)|\dot{\chi}(t)$.